Applied Thermal Engineering 167 (2020) 114761

Contents lists available at ScienceDirect

Applied Thermal Engineering

journal homepage: www.elsevier.com/locate/apthermeng

Thermoelectric generator optimization for hybrid electric vehicles

Wissam Bou Nader*

Groupe PSA, Centre Technique de Vélizy, Vélizy, France

HIGHLIGHTS

- Study assesses the thermoelectric generator auxiliary power unit on hybrid vehicles.
- Exergetic analysis is applied to figure out the thermodynamic configurations.
- Extended range hybrid electric vehicle model is developed.
- The configurations are integrated and vehicle fuel consumption is simulated.
- Recuperative reheat two-stages thermoelectric generator is prioritized.

ARTICLE INFO

Keywords:
Thermoelectric generator
Exergy analysis
Thermodynamic optimization
Extended range hybrid electric vehicles
Fuel consumption

ABSTRACT

Significant research efforts are considered in the automotive industry on the use of low carbon alternative fuels in order to reduce carbon emissions of future vehicles, some of which are only compatible with external combustion machines. These machines are only suitable for electrified powertrains relying on electric propulsion, particularly in range extenders, where the energy converter operates steadily at a constant power at its optimal efficiency. The fuel consumption of these powertrains strongly relies on the performance of the energy converter in terms of efficiency. This paper presents the first study in literature that investigates the potential of fuel savings of an extended range hybrid electric vehicle using a thermoelectric generator system as energy converter substitute to the conventional internal combustion engine. An exergo-technological explicit analysis is conducted to identify the different thermodynamic configurations. An extended range vehicle model is considered and the different configurations are integrated as auxiliary power unit. Fuel consumption simulations are performed on the worldwide-harmonized light vehicles test cycle. Results are compared to the reference internal combustion engine operating as auxiliary power unit. The recuperative reheat two-stage thermoelectric generator is selected among numerous identified thermodynamic configurations, offering high efficiency and net specific work, and consequently lower fuel consumption compared to other configurations. This innovative thermodynamic configuration identified through the methodology proposed in this paper has been patented. Also, this study highlights the importance of increasing the thermoelectric generator's module merit factor in order to achieve system efficiency comparable to the internal combustion engine, which makes this energy converter a potential for the implementation in future powertrains with zero carbon alternative fuels.

1. Introduction

As institutions are becoming aware of the damages of greenhouse gases and other emissions, the fight against ICEs and the quest to find new alternatives is becoming more common by the day. Throughout the years, many technologies were adopted, some of which were already available, and some others were developed to fit the desired needs and requirements. In this quest, the interest in external combustion processes has grown, as internal combustion processes limit the range of available usable fuels. External Combustion Gas turbines [1,2], Rankine machines [3,4], Ericsson engines [5,6], thermoelectric generators [7,8], Stirling engines [9,10] and thermoacoustic engines [11] are occupying the center of attention of researchers as they present possibilities for using alternative fuels [12]. However, their applicability in Automotive systems is still limited but in the process of being explored.

This study focuses on the technology of the thermoelectric generator (TEG). As for the simple TEG, it is composed of three main parts as shown in Fig. 1. The first one is the combustion compartment, containing the combustion chamber blower followed by the combustion chamber; the hot exhaust gases head into the hot heat exchanger where

* Corresponding author at: Groupe PSA, Technical Center of Vélizy, Route de Gizy, P.O. Box VV1415, 78943 Vélizy Villacoublay Cedex, France.
E-mail address: wissam.bounader@mpsa.com.

https://doi.org/10.1016/j.applthermaleng.2019.114761
Received 11 August 2019; Received in revised form 30 November 2019; Accepted 2 December 2019
Available online 05 December 2019
1359-4311/

Nomenclature

AC	alternative current
APU	auxiliary power unit
BC	battery charge
CC	combustion chamber
CCB	combustion chamber blower
CCOT	combustion chamber outlet temperature
COP	coefficient of performance of air conditioning system
C_x	vehicle drag coefficient
DC	direct current
DP	dynamic programming
EC	energy converter
ECP	energy converter power
EG	exhaust gases
EMS	energy management strategy
EREV	extended range electric vehicle
HEX	heat exchanger
H_v	fuel low heating value
ICE	internal combustion engine
n1-TEG	simple-stage thermoelectric generator system
n2-TEG	two-stage thermoelectric generator system
n3-TEG	three-stage thermoelectric generator system
M_v	vehicle mass
NEDC	new european driving cycle
P→(or←)	power out (or in)
P	plug-in
$P_{A/C}$	air conditioning system power
P_{APU}	auxiliary power unit net electric power
P_{AUX}	electric auxiliary power
$P_{cooling}$	cabin cooling thermal power
P_{heater}	cabin heater power
P_m	vehicle mechnical power
Q	thermal power (heat)
R-n1-TEG	recuperative thermoelectric generator system
R-n2-TEG	two-stage recuperative thermoelectric generator system
R-n3-TEG	three-stage recuperative thermoelectric generator system
RRe-n2-TEG	two-stage recuperative reheat thermoelectric generator system
Re-n2-TEG	two-stage reheat thermoelectric generator system
S	vehicle frontal area
SHEV	series hybrid electric vehicle
SOC	state of charge (battery)
SS	self-sustaining
TEG	thermoelectric generator
T_c	cold source temperature
T_h	hot source temperature
T_{TEG}	thermoelectric module operating temperature
W_e	electric power
W_{net}	net specific work
WHR	waste heat recovery
WLTC	worldwide-harmonized light vehicles test cycle
ZT	merit coefficient
η	efficiency
$\eta_{OverallTEG}$	overall thermoelectric generator system efficiency
$\eta_{m,c}$	mechanical efficiency of the air conditioning compressor
$\eta_{e,c}$	electric efficiency of the electric machine driven the air conditioning system
ρ	air density

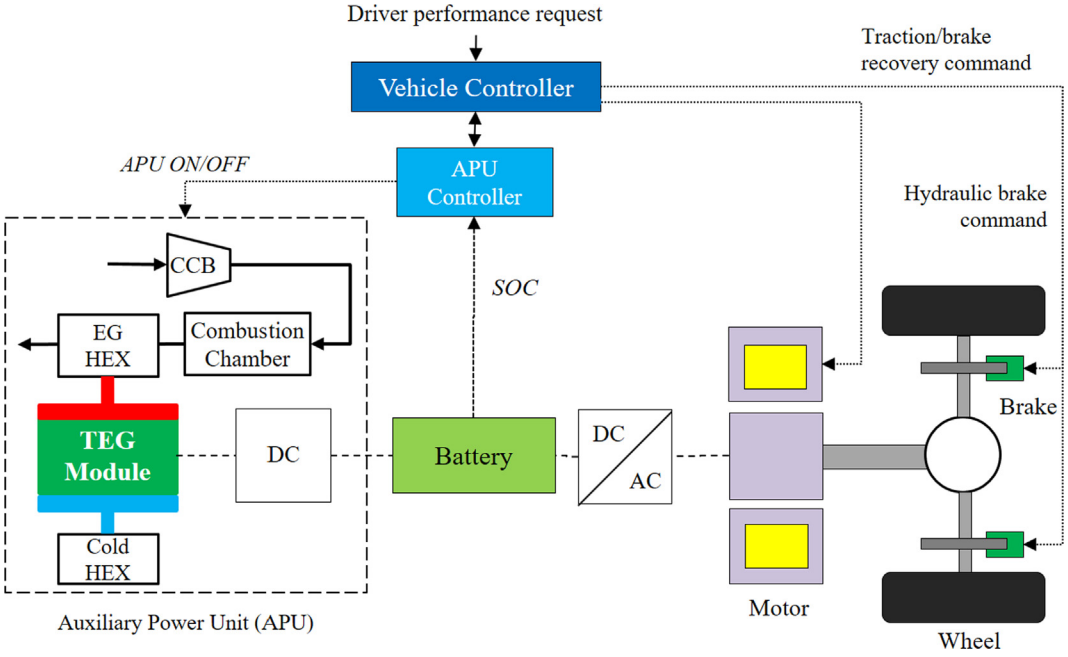

Fig. 1. Configuration of the modeled EREV with a simple external combustion TEG-APU.

they transfer heat to the working fluid through a heat pipe [7]. Following next is the thermoelectric module, which is surrounded by the hot and cold reservoir on each side: this area is the core of the TEG module [13]. The TEG module operates according to the Seebeck effect, where temperature is imposed and constraint the electric load carriers to move from the hot toward cold zones, generating therefore an electric current [14]. Finally, the cold reservoir exchanges heat through the cold HEX, with the ambient air. This ambient air is slightly heated to 50 °C, and can serve as waste heat recovery (WHR) system for the heating of the vehicle, replacing and/or complementing the electric heater. In addition, the TEG module, uses specific material and serves to produce an electric power when operating under a temperature difference between the hot and the cold HEX. Possible candidates for this thermoelectric modules could be elements picking up thermal heat and

transforming the heat power into electrical power like a thermocouple, or quite differently, a material serving as Peltier effect [13,14]. The thermoelectric work output is nothing else than pure electric power, suitable for use in future hybrid electric powertrains, more specifically extended range electric vehicles (EREV) and series hybrid electric vehicles (SHEV).

These systems have been used in industrial applications for a long time, such as aerospace [15], cooling systems [16–18], temperature measurement [13] as well as for mobile phone charging or watches [19], and even proposed as WHR on car seats [20]. TEG systems offer silent and free vibration operation and are potentially attractive for WHR on ICE [7] to convert exhaust heat energy directly into electrical energy, thereby reducing fuel consumption. Many numerical modeling [21–23], parametric evaluation and topological studies [24] based on vehicle TEG prototypes were performed. The first attempt to apply a thermoelectric generator in cars was developed in the University of Karlsruhe in Germany in 1988 [25]. A thermoelectric generator using Bi2Te3 for truck diesel engines was built and tested by Hi-Z Technology Incorporation in the United States in the 1990 s, and a 1 kW generator was tested in 1995 [26,27]. BMW tested many thermoelectric generators prototypes. In 2003, an experimental prototype produced 80 W and the first vehicle prototype was in 2009 producing around 200 W, with a merit coefficient (ZT) of 0.4 and 2% efficiency [28]. In 2011, BMW tested a WHR TEG capable of producing 750 W of electric power. During the same year, another prototype on a different vehicle produced more than 600 W of electricity [29] and achieved a fuel saving of 5% during motorway use. Fiat investigates the TEGs on Iveco light duty vehicles [30] using 270 °C maximum working temperature material. Results show 4% of fuel economy improvement over the WLTC. Honda investigated the TEG technology on F1 vehicle [31] and particular vehicles [32]. Tests were performed with low and high material and with insulating the exhaust line. A 450 W of electric power were produced and results show a 3% of fuel economy. French government funded partially the Renoter project in 2011 [33,34], which brings together eight partners and three laboratories. The TEG power target for passenger car was 100 W on NEDC, 300 W at constant speed of 100 km/h and 500 W at constant speed of 120 km/h [34]. Testing shows that 50We to 100We were recovered with Diesel engine on NEDC and between 80We to 160We on customer cycle.

This study presented in this paper, however, offers for the first time, the replacement of the ICE with an external combustion TEG, to be integrated in an EREV. These powertrains combine a thermal and an electric powertrain in a series energy-flow arrangement [1,35–36]. The thermal powertrain in this study consists of a TEG-system and is referred to as the Auxiliary Power Unit (APU). It operates steadily at the optimum efficiency and mainly used to recharge the battery. The electric powertrain provides the necessary traction power to overcome the driving load. It has also the ability to recover the braking energy during vehicle deceleration. It is important to note that the APU operation is decoupled from the vehicle velocity; therefore, the TEG is designed to meet its best efficiency during all vehicle operating conditions. Fig. 1 illustrates the powertrain configuration of the modeled EREV and a simple TEG-APU system.

The system in question is quite interesting, as it offers many advantages compared to the conventional ICE, among them, its flexible geometry, the simplicity, no noise and vibration, the direct current (DC) generation and its capability to operate with different fuels due to the external combustion process. The TEG system offers also the possibility of three-generation machine that allows in fact the coupling of the TEG with a thermoelectric refrigerator module [37]. However, it does present a few drawbacks that prevented it from being the perfect fit for automotive applications, more importantly its low specific power and low overall efficiency due to low merit factor [38,39], the thermoelectric material strength failure [40] as well as the cost of TEG materials [41].

In fact, as mentioned previously, many works, studies, tests and simulations were conducted by different authors and firms, on TEG technologies to be used as WHR systems, or even sometimes as means of refrigeration, some of which made an impact in the field of thermoelectric [20–24,42].

This literature review on the different TEG systems focused on the processes of waste heat recovery, contributing to the improvement of the fuel economy by reducing the loads falling on the engine; all of these findings clearly show great potential in exploiting this technology, yet, so far, they do not tackle the issue of the conventional ICE in itself whereas it heads towards building on it and improving it. The model in Fig. 1 being the basis of the study, several additional configurations can follow by inserting reheat and recuperative processes, including more than one combustion chamber, and increasing the number of thermoelectric stages. Since no previous study has discussed this particular subject, the following gaps and limitations will be underlined in this literature:

- There are no studies considering the integration of the TEG as main energy converter in vehicle powertrains
- There is no specific methodology that leads to selecting the best configuration of a TEG for an EREV. However, previous studies worked on pre-defined TEG systems based on the simplest

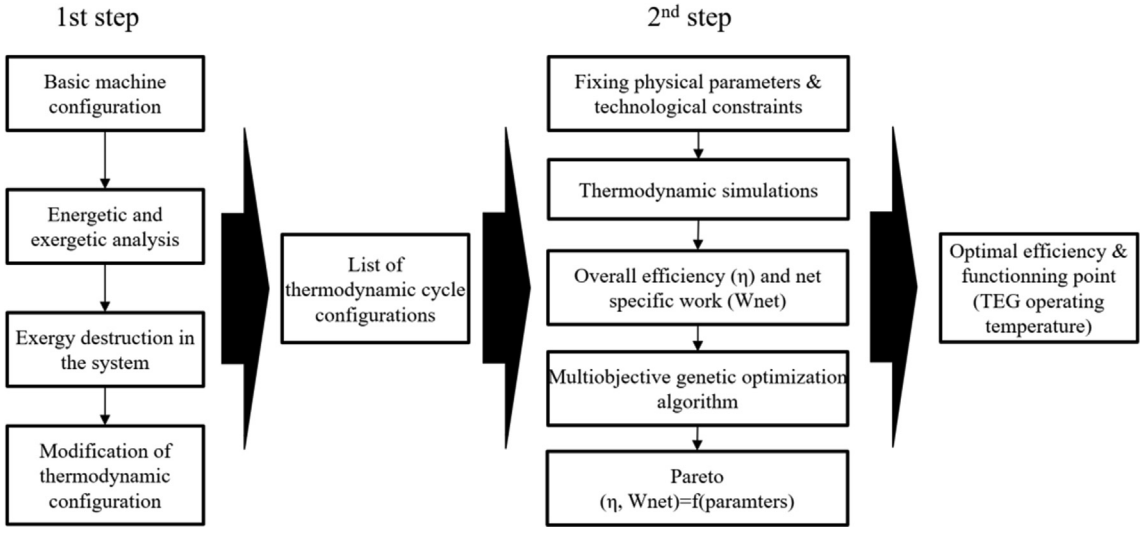

Fig. 2. Exergo-technological explicit selection method of the TEG-system for EREV.

configuration without following any scientific approach in order to choose the right thermodynamic cycle configuration
- There are no studies in the literature that have compared the fuel consumption of an ICE-APU vehicle with a TEG-APU vehicle

Consequently, the lack of research on the issue of replacing the ICE with the TEG, leaves room for this study to present different potential TEG-system options and select the optimal configuration for an EREV application. The objective of this paper is to study the integration of TEG as APU in EREV and to identify the best TEG system thermodynamic configuration. The following section explains in depth the methodology applied for the first time for TEG system for the identification and assessment of these different thermodynamic configurations, based on an exergy analysis within automotive technological constraints. The results are analyzed and synthetized, based on the criterion of the optimal efficiency along with the net specific work produced for three operating temperatures. The third section focuses on the adoption and integration of the different TEG-APU configurations in order to compare them with the conventional ICE-APU in terms of fuel consumption on the Worldwide-harmonized Light Vehicles Test Cycle (WLTC).

This study is novel in two ways: first, it is the first study to consider an exergo-technological explicit analysis for the prioritization and identification of the most efficient TEG-system to be deployed in an EREV among a variety of possible TEG-system options. Second, the study provides a comparative fuel consumption assessment, between EREV of similar performance with TEG-APU and ICE-APU.

2. Methodology for the selection of optimal thermoelectric generator

A specific methodology was adopted in this study, in order to evaluate the potential of the different TEG systems in an EREV. It consisted first and foremost in assessing the system's exergy and optimizing the identified selected configurations while considering technological constraints as will be demonstrated and discussed in the following. This methodology was applied to other energy converters on the same EREV powertrain configuration [1,36].

A detailed plan of the methodology is shown in Fig. 2, following a two-step procedure. The first step relied on exergetic and energetic analyses applied to the simple TEG cycle, in order to get the system efficiency, specific work, and exergy destroyed. These parameters, and mainly looking at the exergy destructions in the system, threw the analysis into deriving the different options and configurations that will allow to optimize the system in terms of exergy losses, by including recuperative processes, as well as combustion chamber reheat and multi-thermoelectric stages, among other plausible options. Accordingly, the list of potential TEG-system configurations is identified.

In the second step, after fixing the physical parameters and the technological constraints, all exergetic and energetic calculations are carried out on all the previously presented configurations resulting in the respective efficiencies, net specific work outputs and TEG operating temperature. Consequently, the optimal combination of work, efficiency and operating point for the different TEG systems is considered for the EREV application, still taking into account realistic physical constraints.

2.1. Energy and exergy analysis of simple thermoelectric generator

This section presents the modeling of the simple TEG system. This system contains two loops: a TEG module loop and a combustion chamber (CC) loop, as illustrated in Fig. 1.

The TEG-loop consists of a TEG module producing a direct current and consequently electric power, operating due to a temperature gradient inflicted by the difference between the hot and the cold HEX. Heat is received from the EG HEX and the heat which was not converted to electric power is rejected through the cold HEX. The CC-loop includes a combustion chamber blower (CCB) and a CC. Both loops exchange heat in the common heat exchanger (EG HEX) component, which serves as hot source for the TEG module.

The TEG system makes use of the Seebeck effect in semiconductors for the direct conversion of heat into electricity [13]. This thermodynamic energy converter is more efficient when operating at high source temperature. The overall conversion efficiency of heat to electricity is expressed according to Eq. (1) which can be also expressed as the cycle efficiency times the heat extraction effectiveness according to Eq. (2).

$$\eta_{OverallTEG} = \frac{P_{net}}{Q_{cc}} \tag{1}$$

$$P_{net} = P_{TEG} - P_{CCB} \tag{2}$$

$$P_{TEG} = \eta_{TEG} * Q_{TEG} \tag{3}$$

$$P_{CCB} = \dot{m} * (H_i - H_o) \tag{4}$$

$$\eta_{OverallTEG} = \frac{P_{net}}{Q_{cc}} = \frac{P_{net}}{Q_{TEG}} * \frac{Q_{TEG}}{Q_{cc}} = \eta_{TEG} * \eta_{Heatextraction} \tag{5}$$

with

$\eta_{OverallTEG}$:Overall TEG system efficiency (%)
P_{net}:Net electric power (kW)
P_{TEG}:TEG system electrical output power (kW)
P_{CCB}:Combustion chamber blower power (kW)
$\dot{m}$:Air mass flow rate (kg/s)
H_i:Enthalpy at the inlet of the combustion chamber blower (kJ/kg)
H_o: Enthalpy at the outlet of the combustion chamber blower (kJ/kg)
Q_{cc}:Heat added in the combustion chamber (kW)
Q_{TEG}:Heat added to the TEG module from the EG HEX (kW)
η_{TEG}:TEG system efficiency ($\eta_{TEG} = \frac{P_{TEG}}{Q_{TEG}}$) (%)
$\eta_{Heatextraction}$:Heat extracted from the hot source ($\eta_{Heatextraction} = \frac{Q_{TEG}}{Q_{cc}}$) (%)

The TEG system efficiency (η_{TEG}) can be expressed as Carnot efficiency times a coefficient which takes into account the Seebeck coefficient (material used), the thermal conductivity and the electric conductivity according to Eq. (6) [13,15,22–23]:

$$\eta_{TEG} = \eta_C * \frac{\sqrt{1 + \frac{S^2}{R_c K} * (\frac{T_h + T_c}{2})} - 1}{\sqrt{1 + \frac{S^2}{R_c K} * (\frac{T_h + T_c}{2})} + \frac{T_c}{T_h}} \tag{6}$$

$$T_{average} = \frac{T_h + T_c}{2} \tag{7}$$

$$Z = \frac{S^2}{R_c K} \tag{8}$$

with

η_C:Carnot cycle efficiency ($\eta_C = \frac{T_h - T_c}{T_h}$)
S:Seebeck coefficient (V/K)
R_c:Electric conductivity (Siemens/m)
K:Thermal conductivity (W/m/K)
T_h:Hot source temperature (K)
T_c: Cold source temperature (K)

he TEG efficiency can therefore be expressed as function of the merit factor ($ZT_{average}$) according to Eq. (9) [13,23]:

$$\eta_{TEG} = \frac{(T_h - T_c)}{T_h} * \frac{\sqrt{1 + ZT_{average}} - 1}{\sqrt{1 + ZT_{average}} + \frac{T_c}{T_h}} \tag{9}$$

An exergy analysis is then carried out as expressed in Eq. (10) [1,36] in order to trace the work losses in the system and their respective amounts, informing on the possible options to reduce the various inefficiencies.

$$E_{in} = [W_{CV}]_{in}^{out} + (E_{out}^{Q} - E_{in}^{Q}) + E_d + E_{out} \quad (10)$$

with

E_{in}:Exergy of the entering flow
E_{out}:Exergy of the leaving flow
$[W_{CV}]_{in}^{out}$:Net Work output
E_{out}^{Q}:Exergy of the heat rejected
E_{in}^{Q}:Exergy of the heat added
E_d:Exergy destruction in the system

The exergy destruction in the CCB is determined using Eqs. (11), assuming no heat exchange with the surroundings.

$$e_{d_{CCB}} = w_{CCB} - (e_{CCB_{outlet}} - e_{CCB_{inlet}}) \quad (11)$$

with

$e_{d_{CCB}}$:Exergy destruction in the combustion chamber blower (kJ/kg)
$e_{CCB_{outlet}}$:Specific exergy at blower outlet (kJ/kg)
$e_{CCB_{inlet}}$:Specific exergy at blower inlet (kJ/kg)

The heat exchanger exergy destruction in the hot HEX the cold HEX is determined using Eq. (12) also by assuming no heat exchange between the HEX and the ambient:

$$e_{d_{HEX}} = [(e_{Hot_{inlet}} - e_{Hot_{outlet}}) + (e_{Cold_{inlet}} - e_{Cold_{outlet}})] \quad (12)$$

with

$e_{d_{HEX}}$:Exergy destruction in the heat exchanger (kJ/kg)
$e_{Hot_{inlet}}$:Specific exergy at the inlet of the HEX hot stream (kJ/kg)
$e_{Hot_{outlet}}$:Specific exergy at the outlet of the HEX hot stream (kJ/kg)
$e_{Cold_{inlet}}$:Specific exergy at the inlet of the HEX cold stream (kJ/kg)
$e_{Cold_{outlet}}$:Specific exergy at the outlet of the HEX cold stream (kJ/kg)

The exergy destruction calculations for the combustion chamber was calculated in this study using Eq. (13), where the average temperature in the combustion chamber is estimated from (14) [43].

$$e_{d_{CC}} = \frac{T_0}{\breve{T}} \cdot \Delta q_{CC} \quad (13)$$

$$\breve{T} = \frac{\Delta q_{CC}}{\Delta s_{CC}} = \frac{h_{CC_{outlet}} - h_{CC_{inlet}}}{s_{CC_{outlet}} - s_{CC_{intlet}}} \quad (14)$$

with

$e_{d_{CC}}$: Exergy destruction in the combustion chamber (kJ/kg)
$\breve{T}$: Average temperature in the combustion chamber (K)
Δq_{CC} : Enthalpy difference in the combustion chamber (kJ/kg)
Δs_{CC} : Entropy difference in the combustion chamber (kJ/kg.K)
T_0 : Reference temperature (K)

Finally, the exergy destruction at the outlet of the system is calculated according to Eq. (15).

$$e_{d_{outlet}} = e_{out} - e_0 \quad (15)$$

with

e_{out}:Exergy at the outlet of the system (kJ/kg)
e_0:Exergy at the reference state (kJ/kg)

After conducting exergy destruction calculations on the system, the basic TEG configuration yielded the results shown in Fig. 3. Four main sources of exergy loss appear on the diagram, occurring mainly in the combustion chamber (41.2%), in the TEG module (25.9%), through the exhaust gases out of the hot HEX (16.1%), and inside the hot HEX (10.1%).

Trying to find solutions for each of these major and minor exergy destruction sources is in fact nothing else than building up the different

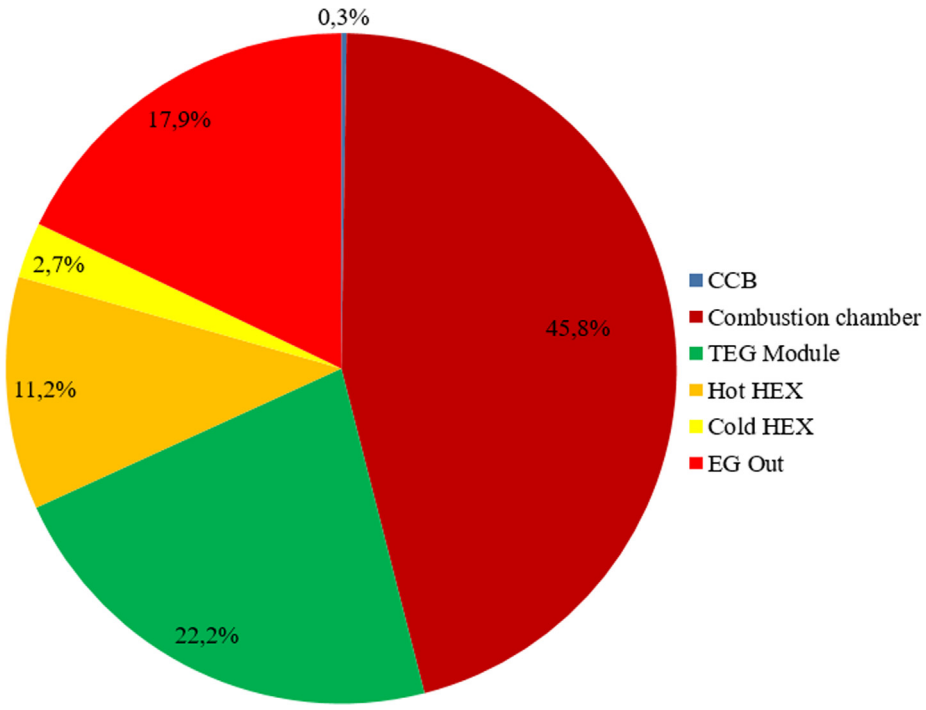

Fig. 3. Distribution of exergy destruction in the simple TEG system with a maximum combustion chamber temperature of 1250 °C, a merit coefficient ($ZT_{average}$ = 4), Hot HEX pinch = 75 K, Cold HEX temperature = 40°, TEG module operating temperature = 450 °C, CCB isentropic efficiency = 80%, reference temperature = 25 °C, reference pressure = 0.1 MPa.

possible configurations to consider for the TEG. Starting first with the combustion chamber, being the highest source of exergy destruction, two options can be considered [1,36]: (1) increasing the combustion chamber outlet temperature within the allowed metallurgic conditions, and (2) increasing the average combustion temperature with either a combustion chamber recuperator or a combustion chamber reheat process.

As for the Exhaust Gases out of the hot HEX, the solution for their exergy destruction lies in the integration of waste heat recovery systems, either in bottoming cycles, or by linking them to the combustion chamber recuperator. The first option relies on using a second or third TEG module in a series arrangement downstream the first module, to transform a part of the thermal heat power to useful electric power. The second option relies on using a recuperator heat exchanger to recover thermal heat in the exhaust to heat upstream the combustion chamber.

Moreover, the thermoelectric module also contributing to the total exergy destruction of the system, would require having its efficiency increased, by increasing the merit coefficient (ZT) in order to reduce the losses.

The last major source of exergy destruction is the hot HEX: reducing its pinch will see its effect also reduce exergy losses, however it requires a higher surface area, and consequently a higher cost and size. As for the minor sources, the cold HEX and the combustion chamber blower also add their contribution to the overall exergy destruction. Increasing the combustion chamber blower efficiency is enough to reduce the exergy losses, where the same goal is served when setting up a WHR process for the cold HEX, however it complicates the system for a low potential of gain.

At this stage, the aforementioned configurations are derived, evaluated and analyzed, in order to choose the optimal solution, based on the potential of exergy losses reduction. Table 1 lists all the proposed system configurations relying on the principles of multi-stage thermoelectric generator cycles, reheat and recuperative processes, following the logic and the trends illustrated in Fig. 4. Furthermore, the respective architectures of the different configurations are represented in Fig. 5 for a better visualization and understanding of the concepts. These figures serve in fact as support for the continuation of the study, as the assessment is carried out on each of the system configurations to get the optimal-realistic architecture, suiting the desired needs and requirements.

2.2. Energy and exergy analysis of identified potential TEG systems

The identified TEG-system options are assessed now in order to prioritize these options based on their respective efficiency and net specific work. The assessment methodology for each option was presented in [1,36]. Systems are modelled using Refprop software [44], using a set of physical parameters such as the combustion chamber maximum temperature, the merit coefficient, the HEX pinches, among others; as summarized in Table 2. These parameters correspond to the state-of-the-art specifications and limitations of TEG component technologies [45,46].

The energy and exergy calculations are made as function of parametric design criteria: the TEG module operating temperature ($T_{TEGi,}$) where (i) denotes the module number, and therefore, the second calculation step uses the multi-objective non-dominated sorting genetic algorithm (NSGA), to determine the Pareto optimal efficiency and net specific work solutions for the optimal ($T_{TEGi,}$) [1,36].

Simulations were performed for three different combustion chamber outlet temperature:

- 950 °C emulating the use of low-cost material
- 1100 °C for medium temperature requiring specific alloys
- 1250 °C high temperature – limit between metallic alloys and ceramic

Fig. 6a, b and c present the exergy losses for 1 kW of net electric power produced from the different considered TEG-systems, operating at optimal efficiency for the three considered maximum combustion chamber outlet temperature (CCOT). Fig. 7a, b and c present the TEG module optimal operating temperature for the three considered maximum CCOT.

The results from these figures confirm the conclusions of Fig. 3, where the main exergy destructions of the simple n1-TEG (Fig. 5a) are in the combustion chamber, in the TEG module and in the exhaust gases at the outlet of the hot HEX. The R-n1-TEG configuration considers adding a recuperator heat exchanger on the upstream of the combustion chamber in order to increase the combustion chamber inlet temperature and reduce the combustion chamber exergy destruction as compared to the n1-TEG. Therefore, the R-n1-TEG presents around 32% less total exergy destruction compared to the n1-TEG when operating at CCOT = 950 °C and 36% when operating at CCOT = 1250 °C. Note that adding the recuperator in the R-n1-TEG results in a decrease on the exergy destruction in the combustion chamber by 47% when CCOT is 950 °C, by 51% when CCOT is 1100 °C and by 53% when CCOT is 1250 °C, compared to the n1-TEG.

In the same way, adding a second TEG module downstream the first module, results in a decrease in the exergy destruction in the exhaust gases at the outlet of the hot HEX, since more heat is recovered and transformed to useful electric power. For instance, according to Fig. 6, the n2-TEG compared to n1-TEG shows 23% less total exergy destruction for all CCOT. This is due to two main reasons: (1) a decrease of the exergy destruction in the EG at the outlet (59% less exergy destruction in the EG at the outlet), and (2) an increase in the first module operating temperature resulting in a total decrease in the TEG module exergy destruction (by 1.5% for all CCOT). The Fig. 7a, b and c highlight the importance of adding the second TEG module. In fact, the n2-TEG first module operates at higher temperature than the n1-TEG module and the n2-TEG second module operates at lower temperature compared to the n1-TEG module. This leads to optimize both the TEG

Table 1
Shortlisting and classification of the different TEG-system options considered in the study.

Category		Simple TEG	TEG w/ Recup	TEG w/ Reheat	TEG w/ Recup & Reheat
I	Single Thermoelectric stage	n1-TEG	R-TEG		
II	Double Thermoelectric stage	n2-TEG	R-n2-TEG	Re-n2-TEG	RRe-n2-TEG
III	Triple Thermoelectric stage	n3-TEG	R-n3-TEG		
With:					
n1-TEG:	Simple-stage TEG				
n2-TEG:	Two-stage TEG				
n3-TEG:	Three-stage TEG				
R-n1-TEG:	Recuperative TEG				
R-n2-TEG:	Two-stage Recuperative TEG				
R-n3-TEG:	Three-stage Recuperative TEG				
Re-n2-TEG:	Two-stage Reheat TEG				
RRe-n2-TEG:	Two-stage Recuperative Reheat TEG				

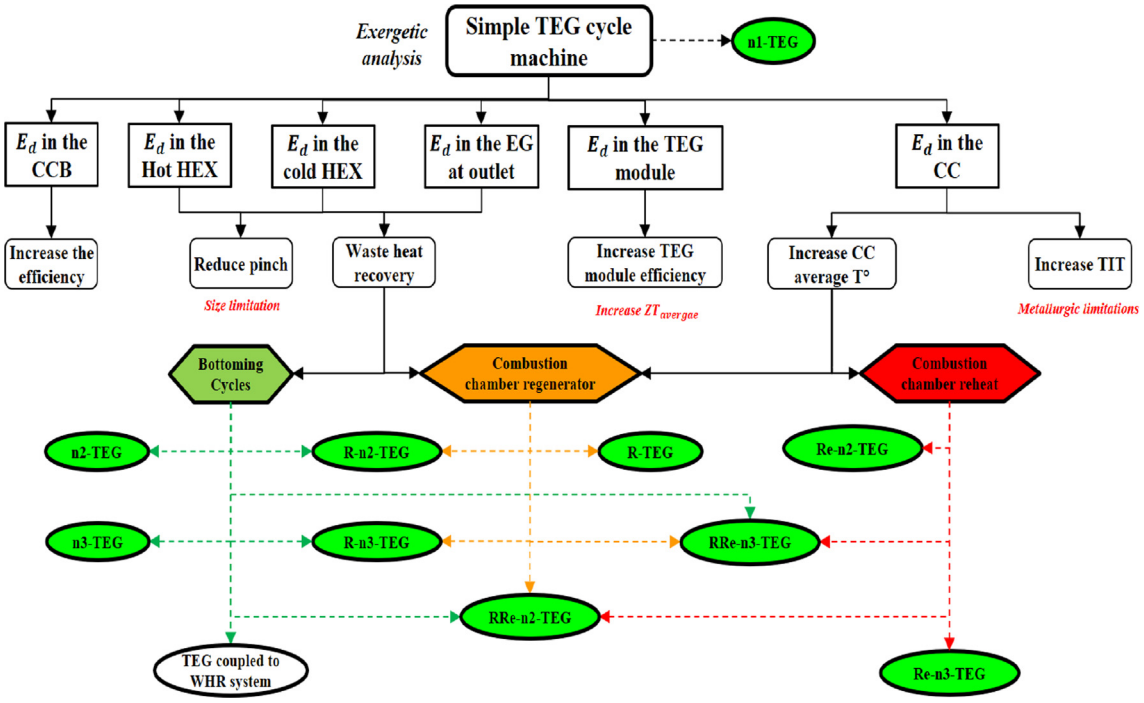

Fig. 4. Exergy assessment methodology for the identification of the TEG-system options with reduced exergy losses.

efficiency as well recovering more heat from the hot source. Adding a third TEG module shows same results but with less relative impact. In fact, the n3-TEG compared to the n2-TEG shows only 8.8% of total exergy destruction reduction and 39% of EG outlet exergy destruction reduction. This affirms that the lower the temperature, the lower the exergy contained-in and the difficult will be to recover this potential of work.

Reheat process is interesting to boost the efficiency of the TEG modules by increasing the module operating temperature. In fact, the Re-n2-TEG shows around 3% less total exergy destruction for all CCOT compared to the n2-TEG. This can be explained, according to Fig. 7a, 7b and 7c where the modules operate at higher temperature, leading to 14.5% less total exergy destruction in the combustion chambers. However, the exergy destruction at the outlet increased, since exhaust gas temperature increased, resulting only in gain of 3% of total exergy losses. To avoid this drawback, the recuperative reheat TEG is the best suited thermodynamic configuration to increase the TEG module operating temperature and to recover the heat at the outlet. Consequently, the RRe-n2-TEG presents 33% less total exergy destruction compared to the Re-n2-TEG.

Fig. 7a, b and c show the optimal operating temperature for the different TEG-systems operating at the three different maximum CCOT. Note that these temperatures are the output of the genetic algorithm optimization, and correspond the best efficiency points selected from the pareto curves presented in Fig. 8a, 8b and 8c below. Compared to a simple TEG system (n1-TEG), adding another TEG-module led to the increase of the optimal operating temperature in the first module. In fact, when operating with one module, the optimal operating temperature is relatively low, which leads to maximizing the heat recovered in the HEX; therefore the optimal efficiency which depends on the amount of heat rejected (the heat extraction effectiveness) and the cycle efficiency is maximum at lower operating temperature. When adding a second module, the first TEG module operates at a higher temperature since the amount of heat remaining is recovered in the second module. When adding a recuperator, and since the heat is recovered by this device, the operating temperature increases as shown in the figures. For instance, for 950 °C CCOT, the R-n1-TEG module optimal operating temperature is 495 °C compared to 366 °C for the n1-TEG. Also, the increase in the CCOT shows an increase in the TEG module operating temperature explained by the higher cycle efficiency due to higher operating temperature. For instance, the R-n1-TEG module operating temperature is 656 °C for 1250 °C CCOT, compared to 577 °C for 1100 °C CCOT and 495 °C for 950 °C CCOT. Same conclusions when comparing the optimal TEG module operating temperature for the other investigated TEG systems.

Based on the above exergy assessment findings, the TEG-systems showing the lowest exergy destruction per 1 kW of net electric power produced will present the highest efficiency. This is reflected in the Pareto curves in Fig. 8a, b and c which illustrate the net specific work versus the efficiency for the investigated TEG-systems for the three different CCOT.

Adding a second TEG module increases the efficiency and the net specific work. In fact, the n2-TEG and the n3-TEG efficiencies are 24% and 34% higher than the n1-TEG respectively for the three operating temperatures.

Also, the n2-TEG and the n3-TEG have 23% and 33% higher net specific work compared to the n1-TEG. This is explained by the additional power recovered when adding another TEG module that recover wasted heat and convert part of it to electric power.

Adding a recuperator shows an increase in the system efficiency. In fact, the R-n1-TEG compared to the n1-TEG has 40% higher efficiency when operating at 950 °C CCOT, 43% at 1100 °C CCOT and up to 45% at 1250 °C CCOT. Also the R-n2-TEG compared to the n2-TEG has 24% higher efficiency when operating at 950 °C CCOT, 26% higher efficiency when operating at 1100 °C CCOT and 27% higher efficiency when operating at 1250 °C CCOT. In the same way, the R-n3-TEG compared to the n3-TEG presents 17.5% higher efficiency when operating at 950 °C CCOT, 18.5% higher efficiency when operating at 1100 °C CCOT and up to 20% higher efficiency when operating at 1250 °C CCOT. These results confirms the benefit of adding a recuperator to recover the waste heat in the EG at the outlet. However, the recuperator presents some drawbacks, mainly a decrease in the system's net specific work. For instance, the R-n1-TEG compared to n1-TEG shows 15% less net specific work when operating at 950 °C CCOT, 11% less net specific work when operating at 1100 °C CCOT and 9% less net specific work when operating at 1250 °C. Also, the R-n2-TEG

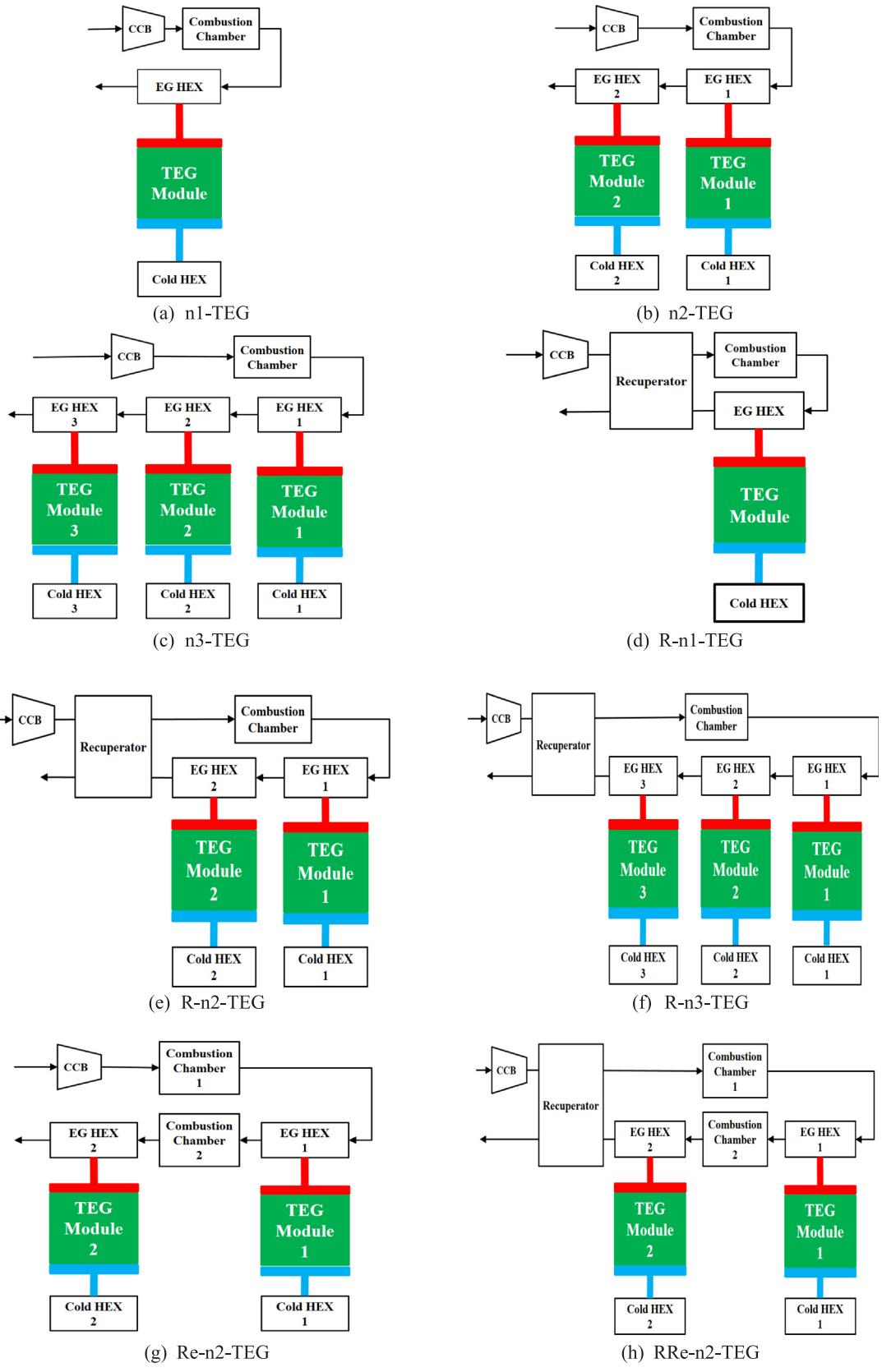

Fig. 5. Configuration of the different TEG-systems considered in the analysis.

Table 2
Simulation parameters based on state-of-the-art component specifications.

Parameter	Unit	Value
Reference temperature	°C	25
Reference pressure	MPa	0.1
CC blower efficiency	%	80
Combustion chambers max T°	°C	950–1100–1250
Combustion chambers pressure drop	hPa	50
Merit coefficient (ZT)	–	4 [45]
Cold HEX temperature	°C	40
Recuperator efficiency	%	85
HEX pinches	K	75
HEXs pressure drop	hPa	75

compared to the n2-TEG has 11.5% less net specific work when operating at 950 °C CCOT, 8.6% less net specific work when operating at 1100 °C CCOT and 6.7% less net specific work when operating and 1250 °C CCOT. In the same way, the R-n3-TEG compared to the n3-TEG presents 10% less net specific work when operating at 950 °C CCOT, 7.7% less net specific work when operating at 1100 °C CCOT and 6.1% less net specific work when operating at 1250 °C CCOT. These results confirm the negative impact of adding a recuperator on the net specific work of the system. In fact, preheating the inlet of the combustion chamber results in a lower net specific work, and consequently higher air mass flow rate for a given net output power, resulting in bigger components, mainly bigger combustion chamber and recuperator heat exchanger.

Results show also that increasing the combustion chamber temperature yields higher system efficiency. In fact, the n1-TEG machine operating at CCOT of 1250 °C shows an increase in efficiency of 11%

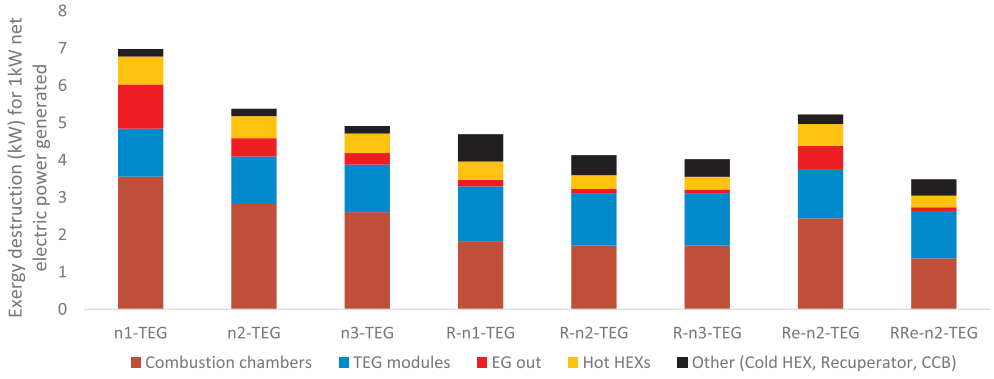

(a) Maximum CCOT = 950°C

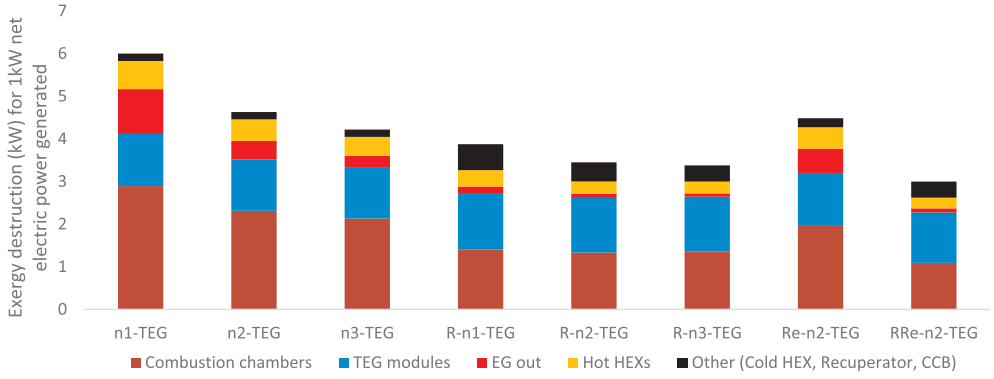

(b) Maximum CCOT =1100°C

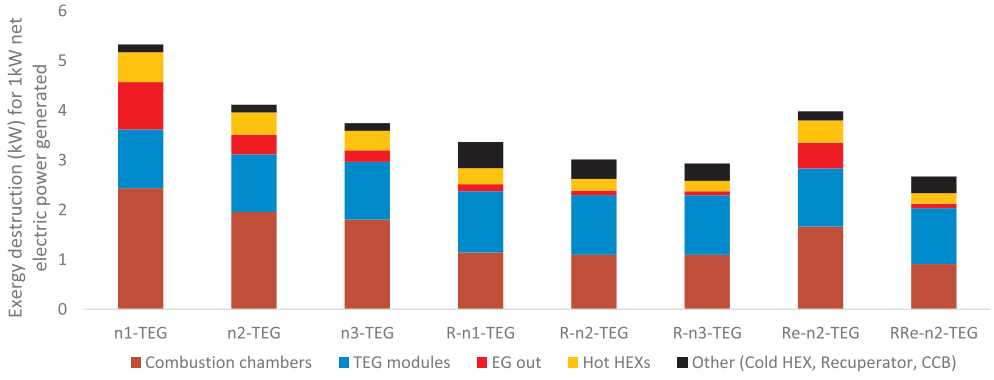

(c) Maximum CCOT =1250°C

Fig. 6. Exergy destruction for 1 kW net electric power delivered from the different TEG systems.

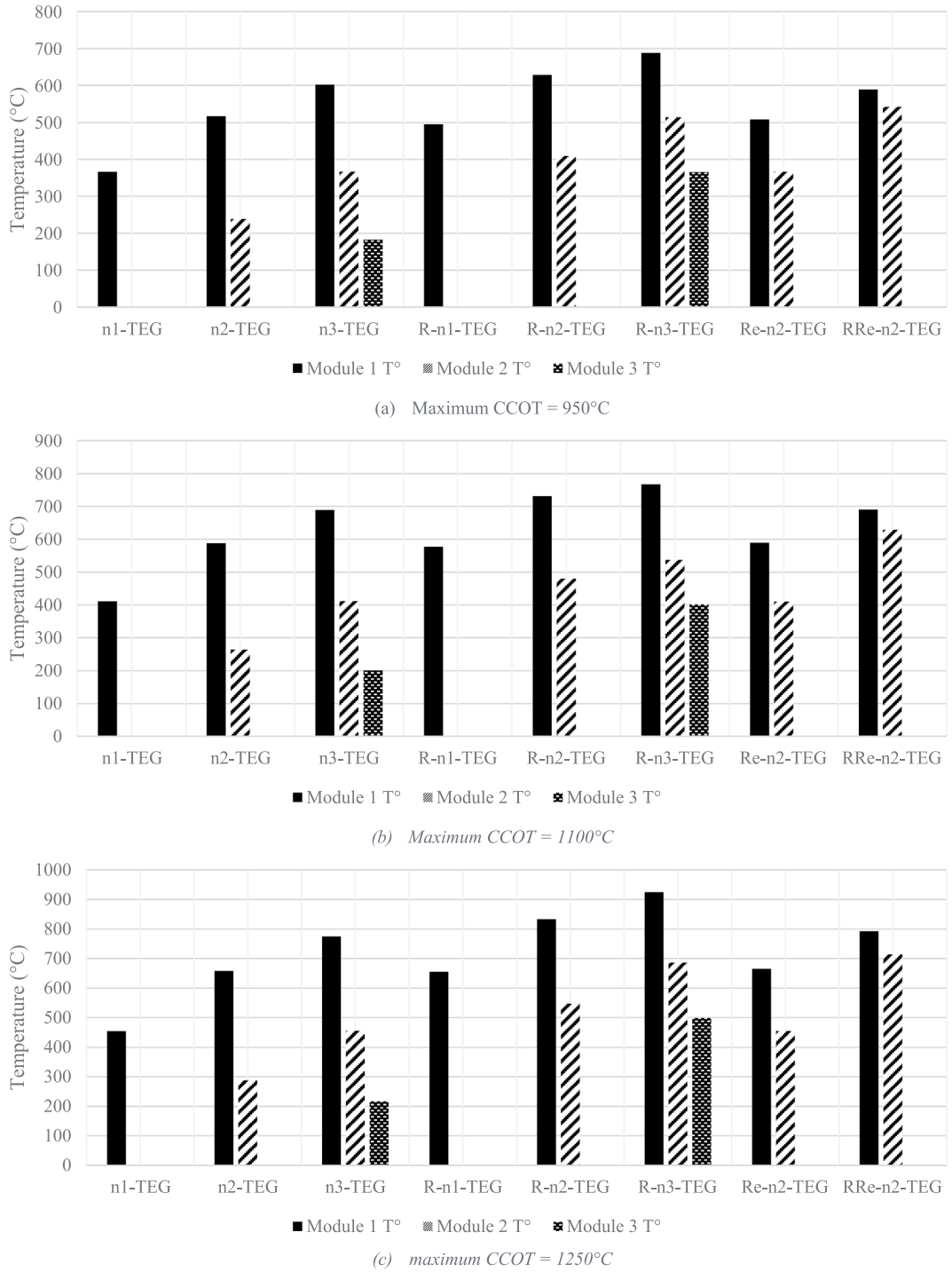

Fig. 7. TEG modules temperature for the different TEG systems operating at their optimal efficiency.

compared to the n1-TEG operating at 1100 °C and up to 26% compared to the n1-TEG operating at 950 °C.

Also, the reheat process is beneficial for increasing both system efficiency and net specific work. In fact, the Re-n2-TEG shows around 27% higher efficiency and 90% higher net specific work compared to the n1-TEG basic configuration. Coupling the reheat process with a recuperator is the best way to boost both efficiency and net specific work. In fact, the RRe-n2-TEG shows a 75% higher efficiency and a 90% higher net specific work compared to the n1-TEG.

The whole assessment process headed towards finding the optimal-realistic configuration to be implemented in the vehicle powertrain. Thus, these three charts in Fig. 8a, b and c are nothing else than the summary of all the investigations and calculations done until now. A clear inspection of the graphs suggests that in the cases of the three distinct operating temperatures, the RRe-n2-TEG machine reveals the best performance in terms of both net specific work and efficiency. As denoted many times, and in order to reduce the complexity of the system to be built and tested further on in the process, the RRe-n2-TEG also demonstrates quite interesting results, being relatively easy to be implemented in a vehicle powertrain.

In the following section, the different TEG systems will be integrated in the EREV and the fuel consumption will be evaluated and compared with the fuel consumption of an ICE operating as APU on the same EREV. Also, while the RRe-n2-TEG demonstrates the higher

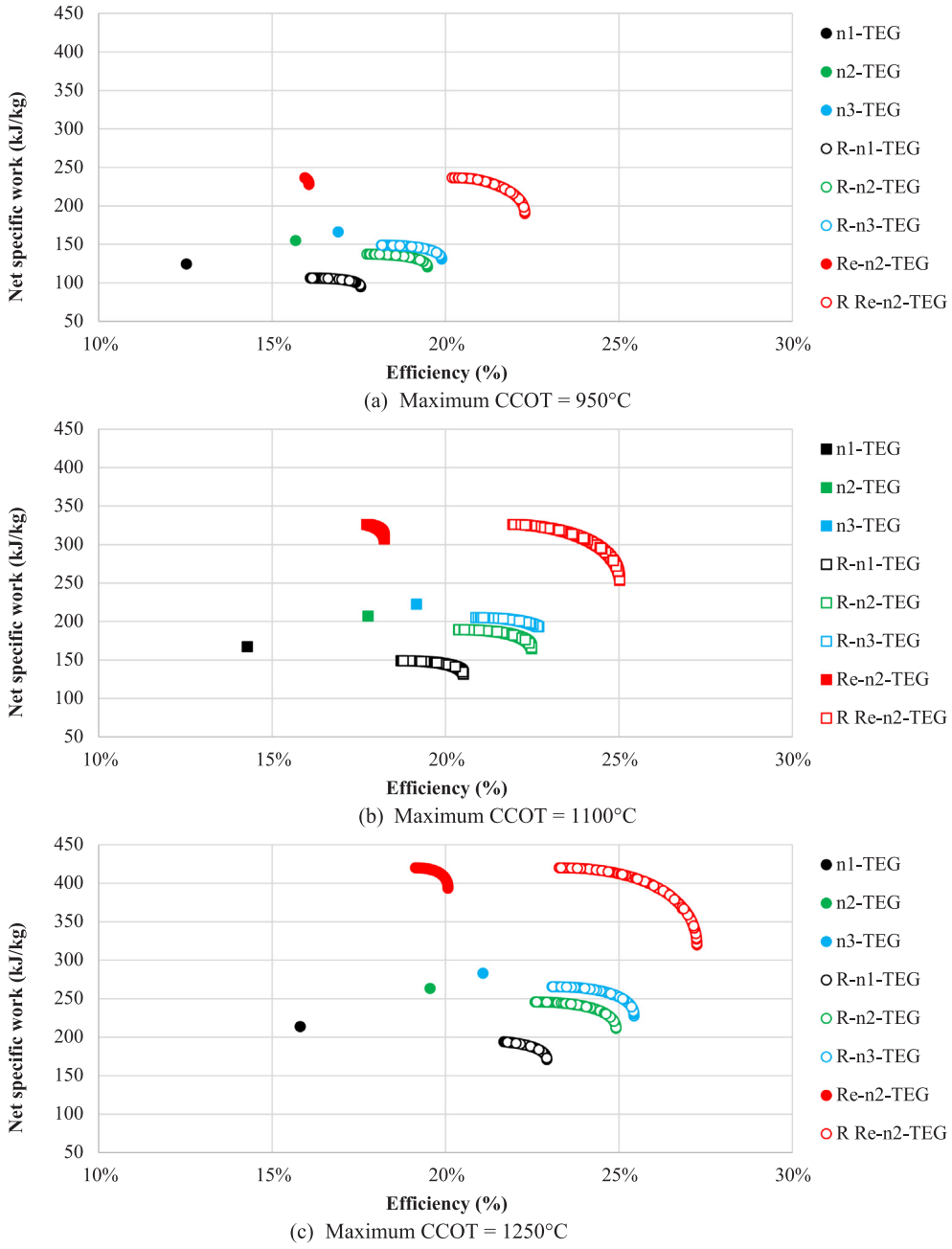

Fig. 8. Pareto Net specific work versus efficiency for the different TEG configurations.

performance, its efficiency remains lower than the today's gasoline ICE which achieve up to 36% of brake efficiency. As shown during this study, the main reason is the low TEG module efficiency due to low merit factor (ZT). Therefore, additional simulations were performed for a high performance machine with merit factor of 10 instead of 4 and a 92% recuperator efficiency instead of 85%. These simulations show that for these considered parameters the RRe-n2-TEG achieve an overall efficiency of 39%, 8.3% higher than the ICE overall efficiency when operating at 1250 °C CCOT. This case will be also considered during EREV fuel consumption powertrain simulations.

3. Vehicle model and energy management strategy

At this stage and having identified the different TEG configuration, the vehicle integration will serve as final assessment step testing the benefits of these systems in terms of fuel economy. As illustrated in Fig. 1, the modeled powertrain consists of a medium-class EREV with series hybrid powertrain forming the TEG-APU complemented by the electric traction system. This powertrain presents the advantage of tackling the main deficiency of Thermoelectric based systems in automotive applications: the transient load. The different TEG systems are designed to operate in this powertrain configuration at steady power corresponding to the optimum efficiency. A summary of the vehicle parameters is presented in Table 3. It is worth mentioning that the weight of the TEG system is considered during the simulations. A power to weight ratio of 125 W/kg is considered. This value is retrieved from [47].

Eqs. (16)–(24) determine the fuel consumption and power flowing between the main components: generator, motor and battery. They also account for the battery current and state of charge, all of which are part of the backward powertrain model of the vehicle. The model calculates the power needs for traction, electric consumption and cabin thermal

Table 3
Vehicle and components specifications.

Vehicle specifications	Symbol	Unit	Value
Vehicle mass (including driver)	M_v	kg	1210
Frontal area	S	m^2	2.17
Drag coefficient	C_x	–	0.29
Wheel friction coefficient	f_r	–	0.0106
Air density	ρ	kg/m3	1.205
Wheel radius	R_w	m	0.307
Auxiliaries consumption	P_{aux}	W	750
Battery maximum power	$P_{b\ max}$	kW	50
Battery capacity	C_b	kWh	20
Battery mass	M_b	kg	356
Battery open circuit voltage	V_{oc}	V	[220, 224, 227, 228, 251]
Battery internal resistance	R_i	Ohm	[0.315, 0.31, 0.31, 0.335, 0.385]
TEG-system power	P_{TEG}	kW	25
TEG efficiency	η_{TEG}	%	Fig. 8c
TEG energy converter mass	M_{TEG}	kg	200
ICE energy converter total mass	M_{ICE}	kg	120
TEG electronic power unit efficiency	η_{le}	%	95
Motor maximum power	P_m	kW	80
Motor maximum efficiency	η_{lm}	%	93
Transmission ratio	i	–	5.4
Transmission efficiency	η_t	%	97
Vehicle total mass	M_t	kg	$M_v + M_b + M_{EC}$[(1)]
Fuel heating value	H_v	MJ/kg	42.5

[(1)]EC = Energy converter ($M_{EC} = M_{TEG}$ or $M_{EC} = M_{ICE}$).

comfort in order to derive the final energy consumption of the vehicle. A detailed model of this powertrain is developed in [1,36].

Eq. (16) assesses the effect of aerodynamic forces, rolling resisting force, inertial force, and vehicle velocity on vehicle traction power requirements:

$$P_{load}(t) = (P_{aerodynamic} + P_{friction} + P_{inertia}) * v(t) = \left(\frac{1}{2}\rho S C_x v(t)^2 + M_t g f_r(v(t)) + M_t \frac{dv(t)}{dt}\right) \times v(t) \quad (16)$$

with

P_{load}:Vehicule traction load (kW)
$P_{aerodynamic}$:Aerodynamic load (kW)
$P_{friction}$:Rolling resistance load (kW)
$P_{inertia}$:Inertial load (kW)
v:Vehicle velocity (m/s)

Through the efficiency of the motor and the transmission, Eq. (17) calculates the traction and braking power of the electric motor:

$$P_m(t) = \begin{cases} \frac{P_{load}(t)}{\eta_t \times \eta_m}, \frac{dv}{dt} \geq 0 \\ P_{load}(t) \times \eta_t \times \eta_m, \frac{dv}{dt} < 0 \end{cases} \quad (17)$$

with

P_m:Electric motor power (kW)
η_t:Transmission efficiency (%)
η_m:Mechanical efficiency (%)

Eq. (18) finds the power provided by the APU when the ICE is on, where $u(t)$ is the APU on/off control variable (0 for off, 1 for on):

$$P_{APU}(t) = u(t) \times P_{TEG} \times \eta_e \quad (18)$$

with

P_{APU}:APU net power (kW)
P_{TEG}:TEG electric power (%)
η_e:Electronic power unit system efficiency (%)

The total powertrain's power which depends on the power of the electric motor power, the auxiliaries, the electric heater and the air-conditioning is provided by Eq. (19). It should be noted that the auxiliaries draw constant power, and the cooling and heating power are as derived by the authors in Reference [48].

$$P_{total}(t) = P_m(t) + P_{aux}(t) + P_{heater}(t) + P_{A/C}(t) \quad (19)$$

with

P_{total}:Total powertrain power (kW)
P_{aux}:Auxiliary power (kW)
P_{heater}:Cabin heater power (kW)
$P_{A/C}$:Air conditioning system power (kW)

where $P_{A/C}(t)$ is equal to:

$$P_{A/C}(t) = \frac{P_{cooling}(t)}{\eta_{m,c} \times \eta_{e,c} \times COP} \quad (20)$$

With

$P_{cooling}$:Cabin cooling thermal power (kW)
$\eta_{m,c}$:Mechanical efficiency of the air conditioning compressor (%)
$\eta_{e,c}$:Electric efficiency of the electric machine driven the air conditioning (%)
COP:Coefficient of performance of the air conditioning compressor

Eq. (21) gives the battery power which is the total power consumed minus the APU power when on:

$$P_b(t) = P_{total}(t) - P_{APU}(t) \quad (21)$$

with

P_b:Battery power (kW)

At this stage, can the battery electric current be calculated by:

$$I_b(t) = \frac{V_{oc}(SOC(t)) - \sqrt{V_{oc}^2(SOC(t)) - 4P_b(t)R_i(SOC(t))}}{2R_i(SOC(t))} \quad (22)$$

$$SOC(t) = SOC_i(t) + \frac{1}{C_b}\int_{t_0}^{t} I_b(t)dt \quad (23)$$

with

SOC:Battery state of charge (%) function of time
C_b:Battery capacity (kW.h)
$I_b(t)$:Battery current (A)

On the other hand, the vehicle fuel consumption can finally be computed with Eq. (24):

$$\dot{m}_f(t) = \begin{cases} \frac{P_{TEG}(t)}{\eta_{TEG} \times H_v}, APU: ON \\ 0, APU: OFF \end{cases} \quad (24)$$

with

$\dot{m}_f$:Fuel mass flow rate (kg/s)
H_v:Fuel low heating value (MJ/kg)

The vehicle controller and the APU controller are shown in Fig. 1 where the first deals with keeping the vehicle's performance in accord with the driver's request, and the latter monitors the battery's *SOC* maintaining it in the desired range, by controlling all APU operations. In addition, the vehicle controller's main objective is to have its electric

motor power meet the demand of traction and brake energy recovery, as shown in Eq. (17). As a result, Eq. (25) considers the on/off (or 0/1) variable $u(t)$ in order to control the APU start operations.

The global optimal control strategy of the APU operations led to the implementation of Dynamic Programming schemes [49], deciding on the optimal strategy $U_{opt} = \{u(1), \cdots, u(N)\}_{opt}$ for the scheduled route at each instant t, aiming at minimizing the fuel cost function J described in Eq. (25). Thus, DP computes the optimal fuel mass flow rate $\dot{m}_f(SOC(t), u(t))$, backward from the final desired battery state of charge SOC_f to the initial SOC_i, in the discretized state time space as illustrated in Eqs. (26)–(28). The generic function adopted in this study was taken from reference [50], where $x(t)$ is the battery SOC's state variable, and $u(t)$ is the APU's on/off control variable. In order to ensure that the speed, the power and the SOC are kept within the normal operation range, the resulting optimal APU on/off strategy U_{opt} must not cause the components to violate their relevant physical boundary constraints included in the DP model and illustrated in Eqs. (29)–(36). Note that the impact of rule-based energy management strategies currently used on hybrid vehicles on the consumption are excluded due to the use of DP as APU energy management strategy. Hence, the fuel consumption results found with DP only depend on the investigated powertrain components as well as their respective efficiencies.

$$J = min\left\{\sum_{t=1}^{N} \dot{m}_f(SOC(t), u(t)) \times dt_s\right\} \tag{25}$$

with

discrete step time: $dt_s = 1$ (26)

number of time instances:

$N = \frac{n}{dt_s}$ (with n the time length of the driving cycle) (27)

state variable equation: $SOC(t+1) = f(SOC(t), u(t)) + SOC(1)$ (28)

initial SOC: $SOC(1) = SOC_i$ (29)

final SOC: $SOC(N) = SOC_f$ (30)

SOC constraint: $SOC(t) \in [0.2,\ 0.9]$ (31)

battery power constraint: $\#\#P_{b_{min}} \le P_b(t) \le P_{b_{max}}$ (32)

motor torque constraint: $P_{m_{min}}(\omega_m(t)) \le P_m(t) \le P_{m_{max}}(\omega_m(t))$ (33)

motor speed constraint $0 \le \omega_m(t) \le \omega_{m_{max}}(t)$ (34)

generator power constraint: $P_{g_{min}}(\omega_m(t)) \le P_g(t) \le P_{g_{max}}(\omega_m(t))$ (35)

generator speed constraint: $0 \le \omega_g(t) \le \omega_{g_{max}}(t)$ (36)

4. Results and discussion

All the calculations, computations and simulations procedures were done for the single purpose of being able to present the TEG machines' advantages or disadvantages in comparison with the conventional ICE. As a result, this section compares the two different EREV configurations of the TEG-APU and the ICE-APU. The TEG systems are designed to operate at their optimal operating point, with an output of 25 kW of mechanical power, which was derived based on vehicle performance constraint and vehicle energetic needs. With this power output, the vehicle is expected to maintain a continuous maximum velocity of 120 km/h without depleting the batteries while ensuring all other no-mechanical energetic needs: auxiliaries, cooling and heating.

As for the ICE-APU, a 1.2 L spark ignition engine with maximum efficiency of 36% was chosen. For both models, gasoline is the fuel used. The simulations are performed on a sequence of one to 10-repeated WLTC (23 km each), covering a driving distance of 230 km. Battery initial and final SOC are 80% and 30% respectively for the Plug-In powertrain configuration, and 60% for both final and initial SOCs for the Self-Sustaining configuration, where the battery capacity chosen is 10 kWh enabling up to 25 km of full electric driving mode. During APU operations, the ICE is allowed to operate at any point of its torque-speed map; however, it was shown that the energy management strategy tends to maximize the powertrain efficiency by operating the engine on its optimal operating line.

Before getting into the fuel consumption analysis, the characteristic of this TEG invited us to conduct a quick autonomy analysis, relying on some basic and simple calculations. This computation required the knowledge of the following characteristics: mechanical power required to propel the vehicle at maximum continuous speed (120 km/h), electric auxiliaries power estimated to be 0.75 kW [48], thermal comfort electric consumption being approximately 1 kW, the generator efficiency, in addition to the SOC_f and SOC_i, and the battery capacity, all found in Table 2. Relating all these parameters using Eq. (37),

$$t(time) = \frac{(SOC_i - SOC_f) * BC}{(Totalpowerconsumption - ECP * efficiency)} \tag{37}$$

where BC is the battery charge, and ECP is the energy converter power, the vehicle operating time can be found for any ECP. In the case of this study, the TEG systems generate 25 kW of electric power without depleting the battery.

This analysis focused on studying one main performance parameter, which is the vehicle's fuel consumption. Two sets of simulations were done in this part, using the DP model on MATLAB, first in order to assess the vehicle's performance with the conventional ICE-APU with a 36% energy converter efficiency, whereas the second set demanded running the simulations for all the considered TEG systems operating at their optimal efficiencies. Only the case of 1250 °C CCOT is considered during the simulations.

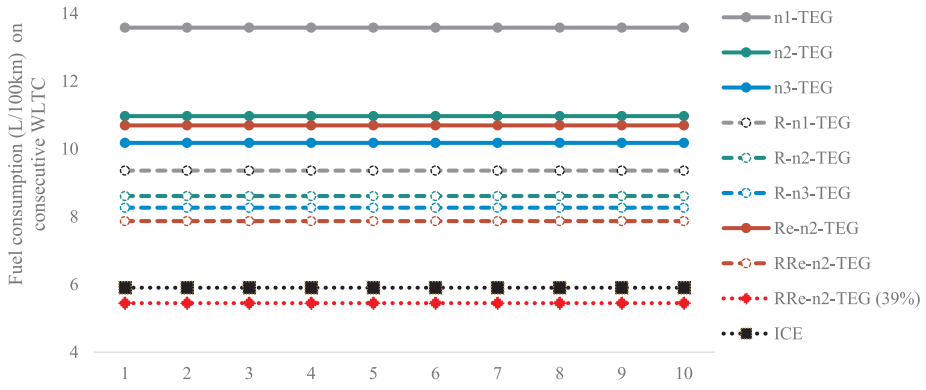

Fig. 9. Fuel consumption on self-sustaining configuration.

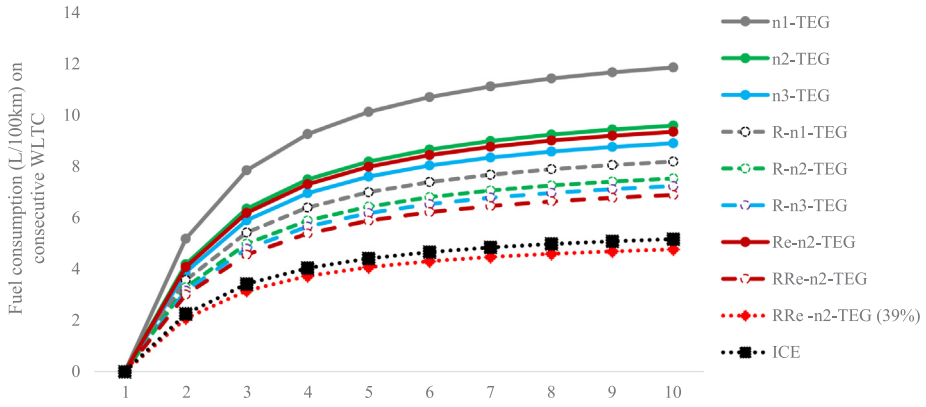

Fig. 10. Fuel consumption on Plug-in configuration.

For each of the engine types, two different SHEV configurations were considered: Plug-in and Self-Sustaining. All the results were extracted and plotted in the graphs shown in Fig. 9 and Fig. 10. In these simulations, (0.75 kW) emulating the need for on-board electric power as considered in addition to the mechanical propulsion needs. Setting all those parameters and conditions, the simulation results were tabulated and plotted, yielding the 2 graphs representing the fuel consumption results in L/km, shown in Figs. 9 and 10, where each graph contains the results of both plug-in and self-sustaining configurations.

A careful inspection of the data, backed by some straightforward calculations, gave a clearer perspective of the TEG fuel consumption behavior and energy converter efficiencies. In fact, each increase in machine efficiency, revealed similar behavior for both scenarios: a decrease in fuel consumption was recorded when comparing the modified TEG systems identified through the methodology proposed in this paper, to the basic n1-TEG configuration. For instance, the n2-TEG shows around 19% of fuel consumption reduction compared to the n1-TEG on both self-sustaining and plug-in configuration, and the n3-TEG records 25% of fuel consumption reduction compared to the basic n1-TEG on both configurations. Also, the R-n1-TEG show up to 31% of fuel consumption reduction compared to the basic n1-TEG configuration. This behavior was manifested regardless of the electric powertrain configuration, and that is, Plug-in or Self-Sustaining.

As discussed in the previous section, the RRe-n2-TEG with the higher efficiency presents the lowest fuel consumption among the other investigated systems, with approximately 42% of consumption saving compared to the n1-TEG.

Further observations should head towards serving the purpose of these graphs and that is, compare the RRe-n2-TEG machine with the ICE. In fact, these graphs are quite demonstrative and illustrative, as they reveal useful information regarding the respective fuel consumptions. It is clearly apparent that the ICE's fuel consumption is lower, hence better, than that of the RRe-n2-TEG even for 1250 ˚C CCOT, undoubtfully improving with an increasing engine efficiency.

Microsoft Excel was used again at this stage, to check for percentage differences in the fuel consumptions for both Plug-In and Self-Sustaining configurations in all scenarios and efficiencies. The trickiest of both configurations seemed to be the Plug-in Hybrid, where there is a range of percentage differences in the cases considered: when the RRe-n2-TEG was operated having a 27% efficiency, the ICE showed to have 33% better fuel economy; regardless of the electric powertrain configuration, and that is, Plug-in or Self-Sustaining.

As the TEG-APU on EREV fuel consumption decreases with an increase in the system efficiency, it is worth mentioning that increasing the TEG module efficiency and its merit factor from 4 to 10 results in a fuel consumption comparable to the ICE. Also 39% TEG efficiency can be achieved when both merit coefficient is increased up to 10 and recuperator efficiency up to 92%, leading to fuel consumption saving up to 7.7% compared to the ICE. This is an important result for scientists working in the field of thermoelectric generators, since this energy converter is proved to be a potential substitute for ICE when the module efficiency is increased.

5. Conclusion

A lengthy process was undertaken in this study in order to reach its main goal, that of exploring the feasibility of replacing the conventional internal combustion engine with a new device, a new technology, and for the first time in the literature, the thermoelectric generator in automotive powertrain application. An energetic and exergetic analysis comes as a first step in order to identify the different possible machine configurations and be able to choose the optimal system for extended range electric vehicles, always taking into account automotive and technological constraints. Consequently, the most suitable device was the two-stage recuperator reheat thermoelectric generator, offering the best performance in terms of efficiency and net specific work. This new innovative thermodynamic configuration proposed in this paper have been also patented. An extended range electric vehicles with a series hybrid powertrain is modeled both in Plug-In and Self-Sustaining modes, and the identified thermoelectric generator configuration and internal combustion engine operating as auxiliary power units are simulated and compared in terms of fuel consumption.

Simulation results revealed 33% higher fuel consumption with the identified thermoelectric generator configuration compared to the conventional internal combustion engine with both Plug-In powertrain, and Self-Sustaining powertrain. However, this study left room for improvements on all levels, since all the calculations were based on the simplest and most intuitive assumptions and procedures when it came to improving the system efficiency. Focusing once again on the efficiency improvements possibilities, that of the system components for example, from the heat exchanger's, to the combustion chamber, to the thermoelectric generator modules and etc., the identified system could achieve efficiencies higher than 36%, going up to 39%. Last stage simulations were done, adopting the same strategies as in previous runs, assessing the vehicle's fuel consumption with a 1250 ˚C combustion chamber outlet temperature of 39% efficiency, achievable with a merit coefficient of 10 and a recuperator effectiveness of 92%. After the data were extracted and tabulated, promising results showed better vehicle fuel economy of the thermoelectric generator auxiliary power unit when compared to the internal combustion engine auxiliary power unit.

The percentage differences in this case appeared to be positive for the thermoelectric generator, as it demonstrates better fuel economy when having an efficiency of 39%. With the Plug-in configuration and the self-sustaining one, the differences is about 7.7% of additional fuel consumed by the internal combustion engine.

CRediT authorship contribution statement

Wissam Bou Nader: Conceptualization, Methodology, Validation, Visualization, Investigation, Validation.

Declaration of Competing Interest

The authors declared that there is no conflict of interest.

Acknowledgement

This work was done in Groupe PSA - technical center of Vélizy, France. The author would like to thank the support of “Groupe PSA”.

References

[1] W. Bou Nader, C. Mansour, M. Nemer, Optimization of a Brayton external combustion gas turbine system for extended range hybrid electric vehicles, Energy (2018).
[2] Kautz Martin, Hansen Ulf, The externally fired gas turbine (EFGT-Cycle) for decentralized use of biomass, Applied Energy (2007).
[3] Qiu Guoquan, Liu Hao, Riffat Saffa, Expanders for micro-CHP systems with organic Rankine cycle, Appl. Therm. Eng. (2011), https://doi.org/10.1016/j.applthermaleng.2011.06.008.
[4] Marcio Santos, Jorge André, Sara Francisco, Ricardo Mendes, José Ribeiro, Off-design modelling of an organic Rankine cycle micro-CHP: Modular framework, calibration and validation, Appl. Therm. Eng. 137 (June 2018).
[5] S. Bonnet, M. Alaphilippe and P.Stouffs, Energy, exergy and cost analysis of a micro-cogeneration system based on an Ericsson engine, Int. J. Therm. Sci. 10.1016/j.ijthermalsci.2005.09.005.
[6] N.P. Komninos, E.D. Rogdakis, Design considerations for an Ericsson engine equipped with high-performance gas-to-gas compact heat exchanger: a numerical study, Appl. Therm. Eng. 133 (March 2018).
[7] B. Orr, A. Akbarzadeh, M. Mochizuki and R. Singh, A review of car waste heat recovery systems utilizing thermoelectric generators and heat pipes, Appl. Theram. Eng., 101, 2016.
[8] K. Qiu, A.C.S. Hayden, Integrated thermoelectric and organic Rankine cycles for micro-CHP systems, Appl. Energy (2012), https://doi.org/10.1016/j. apenergy.2011.12.072.
[9] A. Aliabadi Amir, J. Thomson Murray, S. Wallace James, Tzanetakis Tommy, Lamont Warren, Carlo Joseph Di, Efficiency and emissions measurement of a stirling-engine-based residential microcogeneration system run on diesel and biodiesel, Energy Fuels (2009), https://doi.org/10.1021/ef800778g.
[10] Ulloa Carlos, Porteiro Jacobo, Eguia Pablo, Jose M. Pousada-Carballo, Application model for a stirling engine micro-generation system in caravans in different european locations, Energies (2013), https://doi.org/10.3390/en6020717.
[11] M. Petach, E. Tward, S. Backhaus, Design of a high efficiency power source (HEPS) based on thermoacoustic technology, 2004. Final report, NASA contract no. NAS3e01103, CDRL 3f.
[12] R. Cracknell, G. Kramer, E. Vos, Designing fuels compatible with reformers and internal combustion engines, SAE Technical Paper 2004–01-1926 (2004), https://doi.org/10.4271/2004-01-1926.
[13] P. Wang, B.L. Wang, J.E. Li, Temperature and performance modeling of thermoelectric generators, Int. J. Heat Mass Transf. 143 (2019).
[14] U. Gottlieb, et al., Magnetic properties of single crystalline Mn4Si7, J. Alloy. Compd. 361 (1–2) (2003) 13–18.
[15] D.M. Rowe, Thermoelctrics Handbook: macro to nano. 2006: CRC/Taylow & Francis.
[16] L. Lin, Yu-Feng Zhang, Hai-Bo Liu, Jing-Hui Meng, Wei-Hsin Chen, Xiao-Dong Wang, A new configuration design of thermoelectric cooler driven by thermoelectric generator, Appl. Therm. Eng. 160 (2019).
[17] H.K.O. Nishihata, T. Ueno, Peltier cooling system utilizing liquid heat exchanger combined with pump. Proceedings of the 21st International Conference on Thermoelectrics. 2002.
[18] M.W.R. Davis, P. Clarke, CPU cooling using high efficiency liquid flow heat exchangers. Proceedings of the 23rd International Conference on Thermoelectrics. 2004.
[19] M.N. Kishi, H. Hamao, T. Yamamoto, M. Sudou, S. Mandai M. Yamamoto, S. Micro thermoelectric modules and their application to wristwatches as an energy source. Proceedings of the 18th International Conference on Thermoelectrics. 1999.
[20] J.W. Fairbanks, Thermoelectric Developments for Vehicular Applications, FreedomCar & Vehicle Technologies Program, U.S Department of Energy, Energy Efficiency and Renewable Energy, August 2006.
[21] Sumeet Kumar, Stephen D. Heister, Xu. Xianfan, James R. Salvador, Gregory P. Meinsner, Thermoelectric generators for automotive waste heat recovery systems part I: numerical modeling and baseline model analysis, J. Electron. Mater. (2013), https://doi.org/10.1007/s11664-013-2471-9.
[22] N. Espinosa, M. Lazard, L. Aixala, H. Scherrer, Modeling a Thermoelectric Generator Applied to Diesel Automotive Heat Recovery, Journal of ELECTRONIC MATERIALS, Vol. 39, No. 9, 2010.
[23] Doug Crane, John Lagrandeur, Vladimir Jovovic, Marco Ranalli, Martin Adldinger, Eric Poliquin, Joe Dean, Dmitri Kossakovski, Boris Mazar, Clay Maranville, TEG On-vehicle performance and model validation and what it means for further TEG development, J. Electron. Mater. 42 (7) (2013).
[24] Horst FRIEDRICH, Michael SCHIER, Christian HAFELE, Tobias WEILER, Electricity from exhausts – Development of thermoelectric generators for use in vehicles, Research Thermal Management, 2010.
[25] U.G.E. Birkholz, U. Stohrer, K. Voss, Conversion of waste exhaust heat in automobiles using FeSi2 thermoelements. Proceedings of the 7th International Conference on Thermoelectric Energy Conversion. 1988.
[26] J.E. Bass, N.B. Leavitt, A. Performance of the 1 kW thermoelectric generator for diesel engines. In proceeding of the 13th Inthernational Conference on Thermoelectrics. 1995. AIP Conf. Proc. New York.
[27] John C. Bass, Aleksandr S. Kushch, Norbert B. Elsner, Thermoelectric generator (TEG) for heavy diesel trucks Hi-Z technology, Int. Thermoelect. Soc. (2006).
[28] J. Liebl et al., Der thermoelektrische Generator von BMW macht Abwärme nutzbar. In: MTZ 70 (2009), Nr. 3, S. 272-281.
[29] Boris MAZAR, State of the Art Prototype Vehicle with a Thermoelectric Generator, BMW Group, TE Application Workshop, Baltimore, March 21st 2012.
[30] Will Hornick, “Case Study Fiat: The First Light Commercial Vehicle Equipped with a Thermo-Electric Generator”, 2013.
[31] Richard Stobart, Dan Milner, The potential for thermo-electric regeneration of energy in vehicles, SAE International 1333 (01) (2009).
[32] Masayoshi Mori, Takeshi Yamagami, Mitsumasa Sorazawa, Takatoshi Miyabe, Shunji Takahashi and Tomohide Haraguchi, Simulation of Fuel Economy Effectiveness of Exhaust Heat Recovery System Using Thermoelectric Generator in a Series Hybrid, Honda R&D Co., SAE International 2011-01-1335.
[33] R. Yu, L. Aixala, C. De Vaulx, Waste Heat Recovery by Thermoelectricity on passenger car and heavy-duty truck diesel engine : The RENOTER project, 2012.
[34] Renoter Project, Renault Trucks, 3rd Thermoelectric Applications Workshop : 20-22 March 2012 in Baltimore.
[35] W. Bou Nader, C. Mansour, C. Dumand, M. Nemer, Brayton cycles as waste heat recovery systems on series hybrid electric vehicles, Energy Convers. Manage. (2018).
[36] Wissam Bou Nader, Charbel Mansour, Maroun Nemer and Olivier Guezet, Exergo-technological explicit methodology for gas-turbine system optimization for series hybrid electric vehicles. Proceedings of the institution of mechanical engineers, Part D: journal of automobile engineering, 2017.
[37] Seyed Mohsen Pourkiaei, Mohammad Hossein Ahmadi, Milad Sadeghzadeh, Soroush Moosavi, Fathollah Pourfayaz, Lingen Chen, Mohammad Arab Pour Yazdi and Ravinder Kumar, Thermoelectric cooler and thermoelectric generator devices: a review of present and potential applications, modeling and materials, Energy, July 2019.
[38] L.D. Hicks, M.S. Dresselhaus, Thermoelectric Figure of Merit of a One-Dimensional Conductor, Phys. Rev. B 47 (24) (1993) 16631–16634.
[39] L.D. Zhao, et al., Ultralow thermal conductivity and high thermoelectric figure of merit in SnSe crystals, Nature 508 (7496) (2014) 373.
[40] Y.J. Cui, B.L. Wang, K.F. Wang, Thermally induced vibration and strength failure analysis of thermoelectric generators, Appl. Therm. Eng. 160 (2019).
[41] Saniya LeBlanc, Shannon K. Yee, Matthew L. Scullin, Chris Dames, Kenneth E. Goodson, Material and manufacturing cost considerations for thermoelectrics, Renew. Sustain. Energy Rev. (2014).
[42] Sumeet Kumar, Stephen D. Heister, Xu. Xianfan, James R. Salvador, Gregory P. Meinsner, Thermoelectric generators for automotive waste heat recovery systems part II: parametric evaluation and topological studies, J. Electron. Mater. (2013), https://doi.org/10.1007/s11664-013-2472-8.
[43] S.K. Som, A. Datta, Thermodynamic irreversibilities and exergy balance in combustion processes, Prog. Energy Combust. Sci. 34 (3) (2008).
[44] G. Morrison, J.S. Gallagher, Refprop : A Thermodynamic Properties Software Program for Refrigerants and Their Mixtures, International Refrigeration and Air Conditioning Conference, Purdue University, 1990.
[45] Bertrand Lenoir, Jean-Pierre Michenaud and Anne Dauscher, Thermoélectricité : desprincipes aux applications, techniques de l’ingénieur, K760.
[46] Kakuei MATSUBARA, Thermoelectric Generator to Utilize Waste Exhaust Heat Energy of Vehicles, Yamaguchi TOKYO University of Science, May 2005.
[47] W.B. Nader, Methodology for the Selection and Optimization of Energy Converters for Automotive Powertrain Applications, Phd thesis, Ecole des Mines de Paris, 2019.
[48] Charbel Mansour, Wissam Bou Nader, Florent Breque, Marc Haddad, Maroun Nemer, “Assessing additional fuel consumption from cabin thermal comfort and auxiliary needs on the worldwide harmonized light vehicles test cycle”, Lebanese American University, Industrial and Mechanical Engineering Department, New York, United States, PSA Group, Centre technique de Vélizy, Vélizy, France, Ecole des Mines de Paris, Center for Energy Efficiency of Systems, Palaiseau, France, published in Elsevier Ltd., 2018.
[49] Mansour C. Trip-based optimization methodology for a rule-based energy management strategy using a global optimization routine: the case of the Prius plug-in hybrid electric vehicle. In: Proceedings of the institution of mechanical engineers. Part D: journal of automobile engineering, vol. 230; 2015. p. 1529e45. Issue 11.
[50] O. Sundstrom L. Guzzella, A generic dynamic programming Matlab function, 2009 IEEE Control Applications, (CCA) & Intelligent Control, (ISIC). St. Petersburg, 2009, pp. 1625–1630. doi: 10.1109/CCA.2009.5281131.